Journal of Molecular Graphics and Modelling 39 (2013) 98–107

Contents lists available at SciVerse ScienceDirect

Journal of Molecular Graphics and Modelling

journal homepage: www.elsevier.com/locate/JMGM

Virtual screening for alpha7 nicotinic acetylcholine receptor for treatment of Alzheimer's disease

Shi-Gao Chen [1], Ruo-Xu Gu [*,1], Hao Dai, Dong-Qing Wei [*]

State Key Laboratory of Microbial Metabolism and College of Life Science and Biotechnology, Shanghai Jiao Tong University, Shanghai 200240, Minhang District, China

ARTICLE INFO

Article history:
Received 16 April 2012
Received in revised form
19 November 2012
Accepted 20 November 2012
Available online 29 November 2012

Keywords:
Alzheimer's disease
Nicotinic acetylcholine receptor
Agonist
Molecular docking
Quantitative structure–activity relationship
Virtual screening

ABSTRACT

Alzheimer's disease (AD) is the most common form of dementia. Although its cause and mechanism of progression are not well understood, various *in vitro* and *in vivo* experiments have proved that the decreased activity of the cholinergic neuron is responsible for the memory damage that is observed in these patients. Therefore, the nicotinic acetylcholine receptor (nAChR) is one of the possible drug targets for this disease. At present, extensive nAChR ligands have been designed, and some of the α7 nAChR agonists (*e.g.*, DMXB-A and JN403) have been found to improve the memories and spatial abilities of animal models. However, most of the α7 nAChR agonists cannot be used therapeutically for various reasons, such as poor selectivity for nAChR subtypes, poor pharmacokinetic properties, or toxicity. In the current study, we built homology models of α7 nAChR and virtually screened possible nAChR ligands by combining molecular docking, molecular feature searches, hydrogen bond analyses, and quantitative structure activity relationship (QSAR) study. Our docking simulations and QSAR modeling were reasonably accurate and predictive of nAChR ligand affinity, and we have provided novel and reasonable computational methods for the virtual screening of possible α7 nAChR agonists that may be effectively used for the treatment of various neural disorders, particularly Alzheimer's disease. The compounds that were found in this study may be assessed in future *in vitro* or *in vivo* experiments for their affinities to nAChRs in addition to their biological functions.

1. Introduction

Alzheimer's disease (AD) is the most common form of senile dementia in the elderly population, affecting increasing numbers of people in recent years. It is a progressive, degenerative neuronal disease that is characterized by the accumulation of senile plaques and neurofibrillary tangles in the brain [1]. The cause and progression of AD are still not well understood, but several hypotheses have been proposed. The oldest and most competitive one is the cholinergic hypothesis, in which the reduction of the neurotransmitter acetylcholine in patients is the main reason for AD [2]. Acetylcholine is the endogenous agonist for the nicotinic acetylcholine receptors (nAChRs), which are members of the Cys-loop ligand-gated ion channel superfamily that act as cation channels at the pre- or post-synapse of the neuron or at the neuromuscular junction to stimulate action potentials and muscle contractions, respectively [3]. In the cholinergic hypothesis, the nAChR is not fully activated by the reduced acetylcholine concentrations, and the resulting low cholinergic neuronal activity is the main reason for the patients' memory damage. Another widely accepted theory is the amyloid hypothesis, which argues that the accumulation of the Aβ amyloid results in senile plaques and neurofibrillary tangles in the brain, and the interaction between the Aβ amyloid and nAChRs induces neural apoptosis and memory impairment [4].

There are extensive nAChR subtypes that are distributed in nearly all types of human tissues, with the α4β2 nAChR and α7 nAChR being the most abundant in the brain [5]. *In vivo* experiments have proven that the α7 nAChR agonists significantly improve the memories and spatial abilities of animal models [6,7]. The current accessible drugs for the treatment of Alzheimer' diseases are all α7 nAChR agonists that are based on the cholinergic hypothesis. The α7 nAChR agonists not only function as substitutes for acetylcholine but also protect the neurons from apoptosis by reducing the toxicity of the Aβ amyloid. The binding of the Aβ amyloid with the α7-type receptors alters the α7 nAChR structure and induces neuronal apoptosis. However, the α7 nAChR agonists prevent the Aβ amyloid from interacting with α7 so that neuronal apoptosis is inhibited [8]. Therefore, the design of novel α7 nAChR agonists is one strategy for the treatment of Alzheimer's disease. For instance, the selective α7 nAChR agonist DMXB-A, which is an analog of

* Corresponding authors at: State Key Laboratory of Microbial Metabolism and College of Life Sciences and Biotechnology, Shanghai Jiao Tong University, 800 Dongchuan Road, Shanghai, Minhang District, China. Tel.: +86 21 34204573; fax: +86 21 34204573.
E-mail addresses: mircial@sjtu.edu.cn (R.-X. Gu), dqwei@sjtu.edu.cn (D.-Q. Wei).
[1] The first two authors make equal contribution to this paper.

1093-3263/$ – see front matter © 2012 Elsevier Inc. All rights reserved.
http://dx.doi.org/10.1016/j.jmgm.2012.11.008

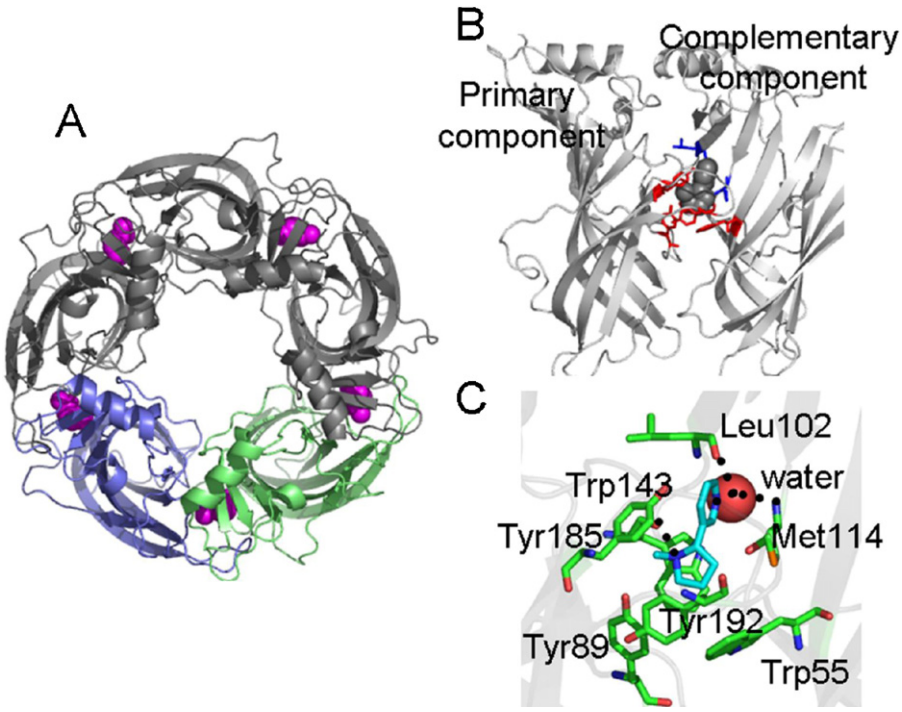

Fig. 1. Conserved interactions between agonist and nAChR: interactions between nicotine and AChBP as an example. Panel A shows the structure of AChBP, which is homologous of the extracellular domain of nAChR. The AChBP is shown in cartoon model with two subunits in light blue and light green, respectively, whereas the other three subunits in gray for clarify. The ligands binding at the subunit interfaces are shown by space filling model in magenta. Panel B is the interactions between nicotine and AChBP. The residues constituting the aromatic cage from the primary component is shown in red in stick model, whereas the residues forming hydrogen bonds with nicotine from the complementary component is shown in blue. The nicotine is shown in gray in space filling model. Panel C shows the details of cation–π interactions and hydrogen bonds. The cationic center of nicotine forms hydrogen bonds with the aromatic cage constituted by Tyr89, Trp143, Tyr185, and Tyr192 from the primary component and Trp55 from the complementary component. The pyridine nitrogen forms hydrogen bonds with the backbone of Leu102 and Met114 *via* a water molecule. The cationic center also forms hydrogen bond with the Trp143 backbone oxygen. These hydrogen bonds are labeled by dashed lines. The carbon atoms of the residues and nicotine are shown in green and cyan, respectively, whereas the nitrogen and oxygen atoms are shown in blue and red. The figure is drawn based on the AChBP-nicotine complex crystal structure (PDB ID: 1UW6).

anabaseine, is under Phase II investigation for Alzheimer's disease [9]. Another α7 nAChR partial agonist, R3487/MEM3454, and its structurally related molecule, MEM-63908, are also under development for the treatment of Alzheimer's disease [10,11]. There are many other α7 nAChR agonists that have been established by *in vivo* experiments to improve the memories and spatial abilities of animal models that cannot be used as drugs because of their toxicities or poor pharmacokinetic properties; *e.g.*, JN403, TC-1698, ABFF, *etc.* [12–14].

Current studies involving the nAChRs, and particularly the rational design of drugs targeting these receptors, are facilitated by their 3D structural models. The electrographic structure of the *Torpedo* nAChR (PDB entry: 2BG9) [15] and the crystal structures of the acetylcholine binding proteins (AChBPs) (*e.g.*, PDB entry: 2BYQ), which are homologs of the nAChR extracellular domain, reveal that the nAChRs are pentermics that are composed of five subunits (five α subunits or two α subunits and three β subunits) [16]. The agonist binding site is located at the interfacial region of one α subunit and one non-α subunit, which are referred to as the primary component and complementary component, respectively (Fig. 1A and B) [17]. Extensive studies have been performed to investigate the agonist-AChBP complexes, and some conserved interactions that are crucial for ligand binding and recognition have been revealed, including the cation–π interaction between the agonist cationic center and the aromatic cage in the binding cavity and the hydrogen bonds that are formed between the agonist and residues from the complementary component *via* water molecules (Fig. 1C) [18]; for example, the structure of the nicotine-Ls-AChBP complex (PDB entry: 1UW6) [19]. The positively charged nitrogen (cationic center) of nicotine forms the cation–π interaction with the aromatic cage that is constituted by Tyr89, Trp143, Tyr185, and Tyr192 from the primary component and Trp55 from the complementary component at the binding cavity, whereas the pyridine nitrogen (hydrogen bond acceptor) forms hydrogen bonds with the backbone of Leu102 and Met114 from the complementary component *via* water molecules. The Trp143 backbone oxygen also forms hydrogen bonds with the cationic center to compensate for the positive charge with its partial negative charges and to stabilize the cation–π interaction (Fig. 1C). Unnatural mutagenesis of the corresponding Trp149 residue in the α7 nAChR eliminating this hydrogen bond significantly decreases the agonist binding affinities, suggesting the importance of this hydrogen bonding to ligand binding [20]. Because the aforementioned interactions are highly conserved in nearly all AChBP and nAChR subtypes, they are likely to be useful in drug design. Extensive molecular modeling studies have been employed to screen nAChR agonists and investigate the agonist-nAChR interactions based upon the crystal structures and homology models of AChBP and nAChR. For example, Ulens et al. used AChBP crystal structures to screen α7 nAChR agonists by docking simulations [21]. Huang et al. used molecular docking and free energy calculations to explain the selectivity of agonists for different nAChR subtypes [22].

The nAChR agonists are not only drug candidates for many neuronal disorders, such as Alzheimer's disease, but are also useful for studying the electrophysiological properties of these ion channels. Although ligands with different structural scaffolds have been designed as agonists for different nAChR subtypes, most of them cannot be used therapeutically for various reasons, such as poor selectivity for the different subtypes, poor pharmacokinetic properties and toxicity. To provide novel chemical structures

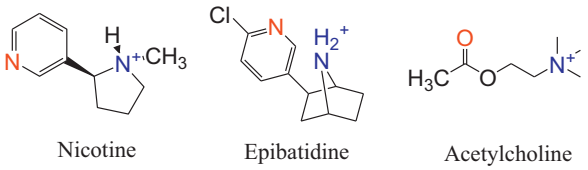

Fig. 2. Structures of three representative α7 nAChR agonists. The cationic center and the hydrogen bond acceptor are labeled by blue and red, respectively. Nearly all nAChR agonists contain these two pharmacophores. (For interpretation of the references to color in this figure legend, the reader is referred to the web version of the article.)

that may be used as nAChR agonist candidates, we employed various molecular modeling techniques, such as homology modeling [23], molecular feature searches, molecular docking, and quantitative structure–activity relationship analyses, in the current study to screen novel α7 nAChR ligands based on the STITCH database. The STITCH database includes the structures of the extensive compounds and information regarding their receptors [24]. We first screened possible nAChR ligands by pharmacophore searches and molecular docking based on the homology model of α7 nAChR. Then, a QSAR model that was based on the structures and affinities of known α7 agonists was constructed and used to further evaluate the docking results. We finally obtained more than one hundred candidates, which may be used in future experiments to investigate their interactions with the nAChRs or to test their effects on the memory abilities of animal models. Our work aimed to find novel candidates that may act as α7 nAChR agonists, which will likely be effective in the treatment of various neural disorders, particularly Alzheimer's disease.

2. Methods

2.1. Virtual screening based on STITCH database

2.1.1. Screening based on molecular features

The purpose of virtual screening in the current study was to find novel α7 nAChR agonist candidates. According to the IUPAC definition, a pharmacophore is "an assembly of steric and electronic features that is necessary to ensure for optimal supermolecular interactions with a specific biological target structure and to trigger (or block) its biological response" [25]. The pharmacophore model that is used in drug design is typically a collection of molecular features and their radii in addition to the distances and angles between them. It has been proven to be of great use in virtual drug screening [26]. As mentioned in the Introduction section, two pharmacophores, including a cationic center and hydrogen bond acceptor, are crucial for agonist binding due to the formation of cation–π interactions and hydrogen bond interactions with the receptor, respectively (Fig. 1). Because they are conserved in various agonists (Fig. 2), it may be helpful to build a model that is based on these two features to search the STITCH database first for agonist-like molecules. In the current study, we used a very simple model consisting of only these two characteristics to search the STITCH database. This model is very simple and may not be suitable as a pharmacophore model. However, because it contains the most important molecular features for ligand recognition, it can be used to rule out the compounds that are not valid nAChR agonists. It could also maintain the structural diversity of the screened compounds because of its simplicity. The results were further screened by Lipinski's "Rule of 5" to exclude compounds that were not suitable to be used as possible drugs [27–29]. The remaining compounds were used in the following molecular docking simulations to evaluate their binding affinities with the α7 nAChR.

2.1.2. Molecular docking and homology modeling

Molecular docking is a method for finding the optimal conformation and orientation of a ligand when it binds to a receptor [30]. We used the molecular docking method to evaluate the binding affinities of the above-screened compounds with the α7 nAChR to further screen for those that have possible interactions with the receptor. The docking simulations were performed using the AutoDock4 package (The Scripps Research Institute, CA, USA) [31]. The compounds were first positioned in the vicinity of the binding site that was located at the interface of the two subunits, and the conformation search was then conducted in a cubic box that was centered on the mass center of the ligand with a length of 15 Å and a grid spacing of 0.375 Å. These parameters were chosen because they were the default parameters of the AutoDock package and were used in our previous studies [32,33] to discern the correct binding conformations of the ligands. For each compound, 100 independent runs were conducted using the genetic algorithm to search for the preferred conformation and orientation of the ligand at the binding site. The structure of the α7 nAChR that was used in the docking simulation was constructed by the homology modeling method, and the description of the homology model may be found elsewhere [32,34].

The homology modeling method is described briefly here. Only the homology model of the extracellular domain of the α7 nAChR was constructed because the agonist-binding site was situated at the subunit interfaces of the extracellular domain. The sequences of the α7 nAChR extracellular domain and Ac-AChBP, which are homologs of the α7 nAChR extracellular domain, were aligned, and the homology model of the α7 nAChR was built based on the crystal structure of Ac-AChBP (PDB entry: 2BYQ) [35] using an in-house program SAMM (Shanghai Molecular Modeling) by the following procedure: (1) the structure of the first α7 subunit was built based on chain A of AChBP by the segment matching method using the other four AChBP subunits as environments; (2) the second α7 subunit was generated based on chain B of the template with the first α7 subunit and the other three AChBP subunits that were used as environments and (3) the remaining three α7 subunits were constructed by the same method. Ten α7 structures were built, and the average structure was calculated and used in the following docking simulations. This homology model was evaluated by the PROCHECK package. It has been used in our previous docking and free energy calculations and has shown excellent accuracy and stability. For example, the secondary structure and the quaternary structure of this homology model were unchanged in our past molecular dynamics simulations, indicating the stability of our model [36]. This homology model was used to study the interactions between JN403, a potent nAChR agonist, and α7 nAChR [33]. The conserved cation–π interactions were found between them and the calculated ligand binding energy of JN403 was consistent with the experimental results, showing the accuracy of our model [33]. Previous virtual screening based on this homology model also found outstanding α7 nAChR agonists [32].

2.1.3. Further screening by hydrogen bond analyses

As previously mentioned, past investigations have found that most of the nAChR agonists formed hydrogen bonds between their cationic centers and the backbone oxygen of Trp149 (one of the residues constituting the aromatic cage in the binding site of α7 nAChR) at the binding cavity (Fig. 1) [18,34]. This hydrogen bonding compensates for the positive charge of the cationic center by the partial negative charge of the Trp149 backbone oxygen and stabilizes the cation–π interaction between the cationic center and the aromatic cage [18]. Therefore, it is critical for agonist recognition and binding. To further evaluate the interactions between the ligands and receptor and screen for the most probable candidates, we analyzed the best docking conformation of each compound to

assess whether this important hydrogen bond exists. A hydrogen bond was considered to be formed when the donor–acceptor distance was smaller than 3.5 Å and the H-donor–acceptor was less than 30°.

2.2. Quantitative structure activity relationship study

To further evaluate the interactions and binding affinities of the compounds that were screened by docking simulations and better understand the physiochemical characteristics affecting the agonists' binding affinities, we then performed quantitative structure activity relationship (QSAR) studies [37]. The molecular structures and experimental binding affinities (K_i values) of 48 known α7 nAChR agonists were collected according to current publications [38–47], and a 2D QSAR model was constructed based on these data. We then recalculated the binding free energies of the compounds that had been selected by the docking simulations using this QSAR model and compared the results with the docking energies to further evaluate the previous virtual screening method. Detailed information describing the dataset that was used in the QSAR studies is included in Supplementary data 1.

2.2.1. Molecular feature calculation

To construct a QSAR model that was based on the binding affinities (K_i values) of the 48 α7 nAChR agonists, a total of 193 molecular descriptors were calculated for each compound based on their energy-minimized structures using SAMM, which is an in-house molecular mechanics and drug design package. These molecular descriptors included both 2- and 3-dimensional descriptors and represented the topological, geometrical, electrostatic and other physicochemical properties of the agonists. Because the descriptor values widely varied and some showed correlations with each other, they were modified before use in the QSAR studies by the following procedure: (1) the descriptors that had the same values for all compounds were removed. One hundred twenty-nine molecular descriptors were retained after this step; (2) the values of these remaining descriptors were normalized in a range from 0 to 1 using the following formula:

$$V_{i\text{-normalized}} = \frac{V_i - V_{\min}}{V_{\max} - V_{\min}}$$

where V_i is the original value of a specific descriptor for compound i, and $V_{\min}$ and $V_{\max}$ refer to the minimum and maximum values of this descriptor among all compounds, respectively. $V_{i\text{-normalized}}$ denotes the final normalized value of the descriptor for compound i.

2.2.2. Molecular feature selection

Because the initial number of descriptors reached one hundred and twenty-nine, it was necessary to delete the highly correlated descriptors and select for those that were most relevant to the agonists' binding affinities to overcome the problem of overfitting when constructing the QSAR model and improving the overall model quality [48]. We used a two-step feature selection method, including the correlation-based feature selection (CFS) method and a wrapper method that is termed GA-SVR (Fig. 3). Correlation-based feature selection (CFS) [49] evaluates the worth of the feature subsets (descriptor subsets) by considering both the individual predictive ability of each feature and the degree of redundancy between the features in that subset, so feature subsets that are highly correlated with the target (the agonists' binding affinities) and have low levels of inter-correlation are preferred. For the CFS procedure, subsets of molecular descriptors were generated first, and their worth values were then calculated by the following equation:

$$r_{zc} = \frac{k\overline{r_{zi}}}{\sqrt{k + k(k-1)\overline{r_{ii}}}}$$

where r_{zc} is the correlation between the summed descriptors in the feature subset and the target (the agonists' affinities), k is the number of descriptors, $\overline{r_{zi}}$ is the average of the correlations between the descriptors in the feature subset and the target, and $\overline{r_{ii}}$ is the average inter-correlation between the descriptors in the feature subset. In this equation, correlation refers to the Pearson's correlation coefficient.

The molecular features that were filtered out by the aforementioned CFS method were further selected for using the wrapper method [50]. In the wrapper method, a feature subset is evaluated by the following procedure: first, a machine-learning algorithm is used to construct a model based on this subset; then, cross validation is used to estimate the accuracy and predictive ability of this model for the agonist affinities. The feature subset that generates the model with the best predictive ability is selected out. In the current studies, the genetic algorithm (GA) [51] was used as the search method to generate feature subsets, and the support vector regression (SVR) [52] method was used as the machine learning scheme to construct a model based on the subsets. The predicted affinities were calculated by 10-fold cross validation based on the model, and the fitness values of the subsets were calculated in terms of the residuals between the predicted and experimental affinities. Thus, this feature selection method is termed the GA-SVR method. The genetic algorithm imitates the evolutionary natural selection process to solve the global optimization problem [53] and is widely used in feature selection [54]. In the genetic algorithm, feature subsets are referred to as individuals and are represented by a sequence of bit string (0, 1), where 1 denotes that the corresponding descriptor is selected in the feature subset and *vice versa* for 0. Individuals with lower predictive errors were considered to be better feature subsets. The parameters of the GA algorithm for each round of feature selection were as follows: the population size of each generation was set at 150, and the maximum generation was set at 100. The crossover probability and mutation rate were set at 0.8 and 0.1, respectively. These parameters have been verified to be suitable for our study.

2.2.3. Model construction and evaluation

We first used the support vector regression (SVR) method to construct our QSAR model for predicting the agonist affinities based on the selected descriptors. Because the agonist affinities (K_i values) are exponentially distributed, their natural logarithms ($\ln K_i$ values) were used as the targets in our QSAR model. The support vector machine (SVM) [55] is a well-known machine learning method that is widely used in data analyses and pattern recognition. It constructs a hyperplane with the largest distance (functional margin) to the nearest training data point of any class because in general, the larger the margin the lower the generalization error of the classifier. If the datasets to discriminate are not linearly separable in a finite-dimensional space, the original space is mapped into a much higher-dimensional space by a kernel function $K(x, y)$, presumably making the separation easier in that space. SVM is suitable for small datasets and shows good performance in many areas [56]. SVM for regression, which is called support vector regression (SVR) [57], was proposed by Vapnik et al. in 1996. Similar to SVM for classification, the model that is produced by SVR depends only on a subset of the training data because the cost function for building the model ignores any training data that is close to the model prediction. In this study, we used the radial basis function (RBF) [58] as the kernel function, and the width of rbfs σ was set at 2.6. Other parameters

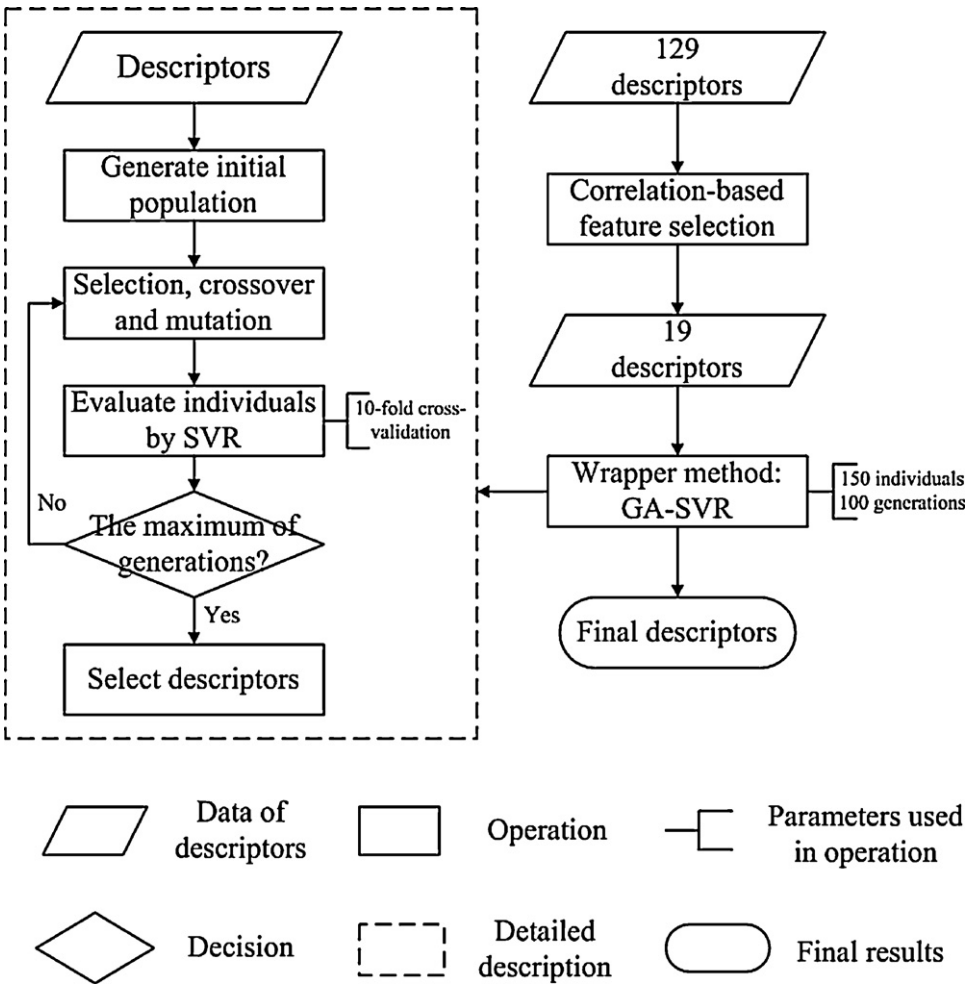

Fig. 3. Flowchart for the process of the feature selection and model building. 4 of the 129 descriptors were selected by the CFS and GA-SVR algorithm and were then used to build a QSAR model using the SVR algorithm.

of SVR, including the values of C and ε, were set at 25 and 0.14, respectively.

We first used leave-one-out cross-validation (LOOCV) to evaluate the performance of our SVR model. LOOCV assigns a single compound from the original sample as the test data and the remaining compounds as the training data. This process was repeated 48 times so that each compound in the sample was used once as the test data. Then, we divided the data set into training sets (36 compounds, 75%) and test sets (12 compounds, 25%) randomly. The training sets were used to construct the SVR model, whereas the test sets were used to evaluate the performance of the model. At last, we obtained the predicted $\ln K_i$ value for each of the 48 compounds based on our SVR model. The SVR model was evaluated by comparing the predicted and experimental affinities.

2.2.4. Comparison of SVR model and docking simulations

To further evaluate the binding affinities of the compounds that were screened for by the docking simulations, we recalculated the binding free energies of the 100 most optimal compounds from the docking results using the QSAR model and compared these results with the docking energies. Because the target of the SVR model was $\ln K_i$, we converted this value to free energy (ΔG) based on the following equation:

$$\Delta G = RT \ln K_i$$

where $R = 8.314\,\mathrm{J\,K^{-1}\,mol^{-1}}$ and $T = 310\,\mathrm{K}$. If the results from the SVR model are in agreement with the docking simulation, then the validity of the virtual screening results is supported.

Although the above regression model could estimate the binding affinities of active compounds (*e.g.*, the best 100 docked compounds) well, it could not discriminate the inactive compounds (*e.g.*, the structures with positive docking energies) from the active compounds because it was constructed based on active agonists. Therefore, we collected some inactive sturctures and built models to discriminate the active structures from the inactive structures based on their physiochemical differences. The resulted prediction model may help us get further understanding of the physiochemical characters affecting the agonists' binding affinities (see Supplementary data 3 for the description of the discriminative model).

3. Results and discussion

3.1. Virtual screening results and data analysis

We first screened the STITCH database according to the following two steps: (1) two molecular features, including a cationic center and a hydrogen bond acceptor, were used for the screening, and then (2) the remaining compounds were further screened by Lipinski's "Rule of 5". Because previous studies have found that all nAChR agonists contain these two molecular features interacting

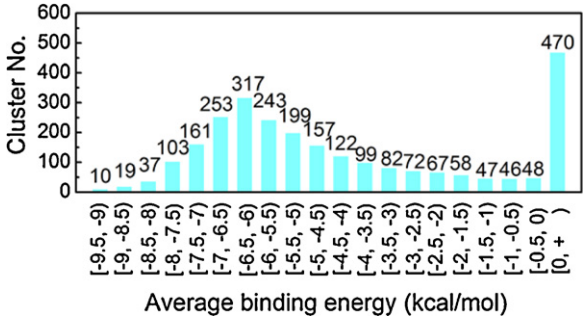

Fig. 4. The distribution of lowest average binding energies obtained by docking 2610 ligands to the α7 nAChR agonist binding site. >75% of the docked compounds (2000) showed average binding energies lower than 0 kcal/mol, whereas ~12% of them (330) have average binding energies lower than −7 kcal/mol.

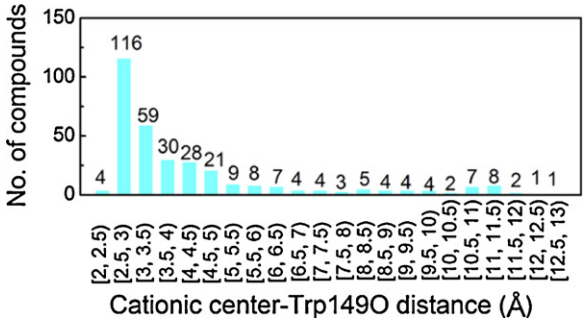

Fig. 5. Distribution of the distances between cationic centers of ligands and Trp149 backbone oxygen in the docked conformations.

with conserved residues at the binding cavities in the structural models of the agonist-AChBP/nAChR complexes (Figs. 1 and 2), they may be crucial for ligand recognition. Therefore, step 1 was used to rule out those that are not agonists. We did not employ a well-defined pharmacophore model to maintain the structural diversities of the screened compounds. Step 2 was used to exclude those that were not suitable for use as drugs. After these two steps, we finally obtained 2610 compounds, which were then used in the following docking calculations.

The docking calculations were based on a homology model of the α7 nAChR extracellular domain. The structure of the homology model and its superposition with template are shown in Supplementary data 2. For each molecule, the preferred conformation and orientation were searched for at the binding site using the AutoDock package, and the binding free energies were calculated by the following equation:

$$U_{\text{binding}} = U_{\text{Intermolecular}} + U_{\text{Internal}} + U_{\text{Torsional}} - U_{\text{Unbound}}$$

where U_{binding} is the estimated binding energy, $U_{\text{Intermolecular}}$ is the interaction energy between the ligand and receptor, U_{Internal} is the internal energy of the ligand, and $U_{\text{Torsional}}$ is the torsional energy of the ligand's rotatable bond. For each compound, 100 independent runs were performed, and the docked conformations were clustered based on their RMSD with a tolerance of 2.0 Å. Then, the average binding energies of the conformations in each cluster was calculated. The lowest average binding energy of each compound was used to evaluate the ligand's binding affinity. The distribution of the lowest average binding energies of all 2610 compounds is shown in Fig. 4. Over 2000 compounds (>75%) show binding energies that are lower than 0, and their distributions resemble the normal distribution.

As described previously, the hydrogen bond between the agonist cationic center and the Trp149 backbone oxygen is crucial for ligand binding. Because this hydrogen bond is found in all agonist-AChBP complexes [59–61], we hypothesized that a potent agonist candidate should form the same hydrogen bonds with α7 nAChR at its binding cavity. Therefore, we further evaluated the docking results by analyzing whether hydrogen bonds are formed between the best-docked conformations of the screened compounds and the α7 nAChR binding site. The definition of the hydrogen bond was described in Section 2. Only the compounds that showed excellent average binding energies (lower than −7 kcal/mol, ~12% of the docked compounds) in the docking simulations were used in this hydrogen bond analysis. We analyzed 330 compounds in total, and Fig. 5 shows the distribution of the distances between the compounds' cationic centers and the Trp149 oxygen atoms at the α7 nAChR binding sites. The distances of 179 compounds are in the range of hydrogen bond interaction. However, only 97 formed hydrogen bonds with the Trp149 backbone oxygen considering both the donor–acceptor distance and ∠H-donor–acceptor angle. One hydrogen bond was revealed in most compounds, whereas six of them (compounds 104, 108, 115, 118, 119, 164) formed two. The structures and docking energies of the 179 compounds are shown in Supplementary data 4 and 5 and are used in the following analyses.

3.2. Quantitative structure activity relationship studies

3.2.1. Molecular descriptor selection

19 molecular descriptors that were highly correlated with the agonist affinities and had weak intercorrelations were filtered out from the initial 129 descriptors by correlation-based feature selection. Then, 4 descriptors were selected out by the GA-SVR method from these 19 descriptors and used in the QSAR studies (Fig. 3). The 4 descriptors and their meanings are listed in Table 1, including the Zagreb index, PEOE_VSA_PPOS, Kier2, and SlogP_VSA1. The Zagreb index and Kier2 are descriptors for molecular topologies, such as the degree of branching, molecular flexibility, and overall molecular shape. The PEOE_VSA_PPOS and SlogP_VSA1 represent the electrostatic and hydrophobic/hydrophilic properties of the molecules, respectively.

Because cation–π interactions between the agonist and electron-rich aromatic cage at the binding site are important, the positive charges of the compounds are crucial for ligand recognition, highlighting the importance of PEOE_VSA_PPOS (Table 1). Because the side chains of the residues constituting the aromatic cage are hydrophobic, the hydrophobicity of the atoms around the cationic center also affect the ligand affinities by hydrophobic interactions, rationalizing the SlogP_VSA1 parameter [62]. The Zagreb index and Kier2 parameters indicate that the shapes and flexibilities of the ligands are also critical to their binding affinities [63,64]. This has not been previously reported and warrants further investigations.

Table 1
The descriptors used in the QSAR model and their meanings.

Name	Meaning
Zagreb	Zagreb index: the sum of d_i^2 over all heavy atoms i, with d_i the number of non-hydrogen atoms to which atom i is bonded
PEOE_VSA_PPOS	Total positive polar van der Waals surface area
Kier2	Second kappa shape index: $(n-1)^2/m^2$ [69]. n is the number of atoms (not counting hydrogen atoms); m is the number of bonds (except bonds to hydrogen atoms)
SlogP_VSA1	Sum of the approximate accessible van der Waals surface area v_i such that the contribution to $\log P(o/w)$ [70] for atom i (L_i) is in (−0.4,−0.2]

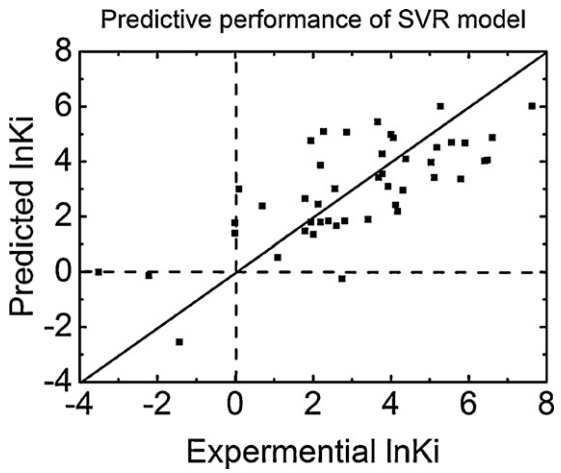

Fig. 6. Predictive performance of the SVR model. The predicted affinities are shown as a function of the experimental affinities. Our QSAR model achieved the predictive accuracy with correlation coefficient of 0.75 and root mean square error (RMSE) of 1.60 kcal/mol.

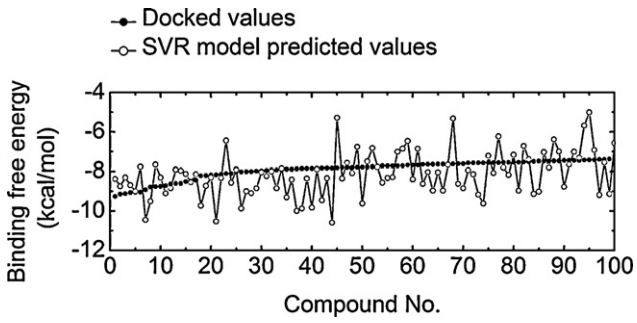

Fig. 7. Comparison of the binding free energies of the docked compounds calculated by QSAR model and the corresponding values obtained by docking calculations. The energy values obtained by two different methods are shown as a function of the compound numbers. The energies calculated by QSAR model fluctuated around the docked energies and they are highly consistent with each other (RMSE of 1.10 kcal/mol).

3.2.2. Predictive ability of QSAR model

The QSAR model was constructed based on the selected 4 molecular descriptors and the experimental affinities of the known agonists by the SVR method. In our model, the radial basis function (RBF) [58] was used as the kernel function. The other parameters were as follows: the width of rbfs σ was set at 2.6, and the values of C and ε were set at 25 and 0.14, respectively. Leave-one-out cross-validation was used to evaluate the predictive performance of our QSAR model. Our model achieved predictive accuracy with a correlation coefficient of 0.75 and root mean square error (RMSE) of 1.60 (Fig. 6). RMSE indicates the average difference between the experimental and predicted $\ln K_i$ values over all compounds and is defined as

$$\mathrm{RMSE} = \sqrt{\frac{\sum (Y_{\mathrm{actual}} - Y_{\mathrm{pred}})^2}{n}}$$

whereas the correlation coefficient between the experimental and predicted agonist affinities is defined as

$$R = \sqrt{1 - \frac{\sum (Y_{\mathrm{actual}} - Y_{\mathrm{pred}})^2}{\sum (Y_{\mathrm{actual}} - Y_{\mathrm{mean}})^2}}$$

where Y_{actual} and Y_{pred} denote the experimental and predicted $\ln K_i$ values, respectively, n denotes the number of compounds, and Y_{mean} denotes the mean of Y_{actual} over all compounds.

In order to further evaluate the predictive ability of our QSAR model, we divided the data set into training sets (75%) and test sets (25%) randomly. The training sets were used to construct the SVR model, whereas the test sets were used to evaluate the performance of the model. RMSE and correlation coefficient of training set are 1.48 ± 0.07 and 0.79 ± 0.03, whereas the corresponding values of the test set are 1.63 ± 0.25 and 0.72 ± 0.10, respectively, implying the reliability of our model again.

To further evaluate the binding affinities of the compounds that were screened by the docking simulations and hydrogen bond analyses, we recalculated the binding free energies of the 100 best docked compounds using our SVR model. Only the 100 most optimal compounds were used because their docked energies were in the same ranges as the affinities of the agonists in the dataset that was used for the QSAR model construction. Thus, the QSAR model may reasonably predict the binding energies of these compounds. The free energies that were obtained by our QSAR model and the corresponding docking energies are displayed in Fig. 7, which shows that the free energy values of the docking simulations and the QSAR model are highly consistent, and the root mean square error is approximately 1.10 kcal/mol. These results indicate the reliability of our virtual screening method and QSAR model.

However, our QSAR model could not be used to discriminate the inactive structures from the active ones. Therefore we constructed a new predictive model to achieve this task based on 48 active agonists with known reasonable binding affinities and 50 ligands without binding affinity. In this model, four molecular descriptors were found to be crucial for the affinities of the agonists (see Supplementary data 3 for the description of this model).

3.3. Analyses of screened compounds

3.3.1. Biological activities of screened compounds reported in literature

Finally, we searched previous publications for reports describing the biological activities of the 179 virtually screened molecules (Supplementary data 5). The six molecules that formed two hydrogen bonds with the Trp149 backbone oxygen all contained a guanidine group (compounds 104, 108, 115, 118, 119, and 164). Compounds 104 and 115 are antihypotensive drugs, whereas compounds 118 and 164 could used to treat metabolic disorders in diabetes and be used as β-adrenergic blockers, respectively. Compounds 6, 14, 17, 19, 24–26, 28, 33, 44, 57, 58, 62–65, 73, 92, 101, 134, 143, 146, 153 and 163 all contain isoxazole rings and could be used as hypothermic, analgesic, anti-inflammatory, and antitussive drugs, *etc.* Compounds 7, 8, 15, 16, 18, 37, 42, 60, 77, 78, 80, 94, 95, 98, 105–107, 111, 114, 125, 130, 135, 136, 142, 148, 149, 158, 159, 161, 165, 167, 168, 173 and 179 may be used as anesthetics or antispasmodics. Compounds 29, 109, 113, and 115 are monoxygenase inhibitors, whereas compound 41 is a sparteine analog contributing to muscle activity. Compounds 82, 147, 154, and 178 are also antihypertensive drugs. Compound 85 may enhance the activities of muscarinic receptors. Compounds 120 and 176 are β-adrenergic blockers. Compound 123 is known as melperone, which is used as an antipsychotic for the treatment of schizophrenia. Compound 138 and 170 are used as antiparkinson's and antiarrhythmic drugs, respectively. Some of the aforementioned compounds, such as the anesthetics, antiparkinson's drugs, and antipsychotic drugs are known to be involved in interacting with the nervous system.

Although the binding affinities of these compounds with α7 nAChR have not been defined, the previously discussed publications suggest the most likely candidates that should be tested first. It has been reported that some anesthetics are blockers or competitive inhibitors of many nAChR subtypes; for instance, curare is a competitive inhibitor of the muscle-type nAChR (α1β1δε

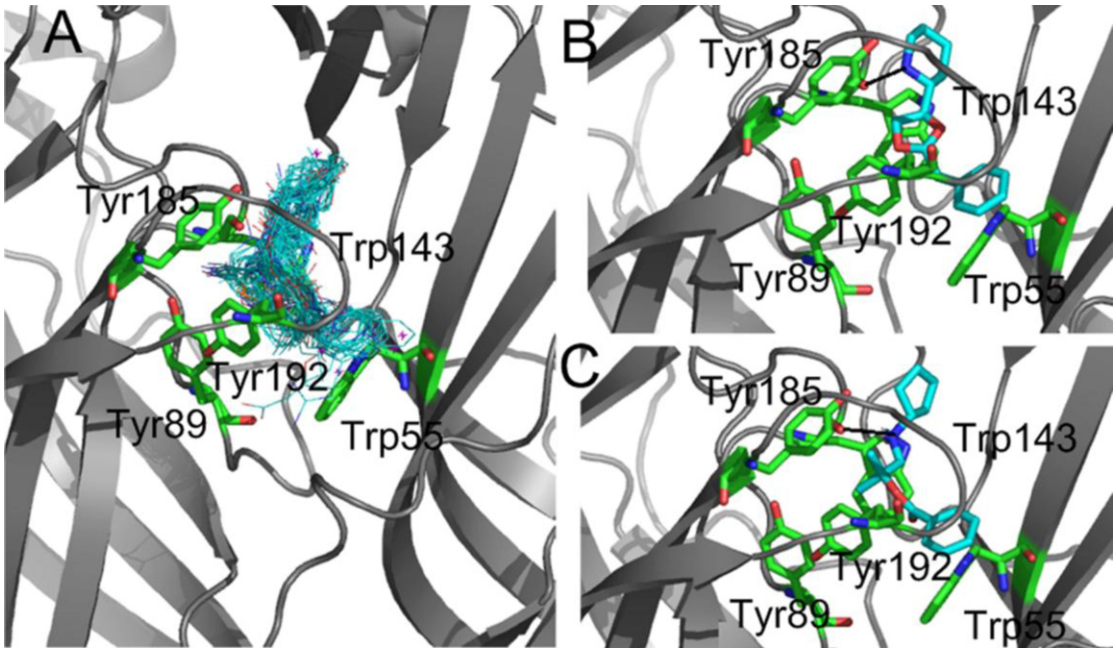

Fig. 8. Interactions between the docked compounds and the α7 nAChR binding cavity. Panel A shows the structures of binding conformations of all the screened compounds. Panel B and C show the binding poses and interactions of compound 18 and 60 at the agonist binding site, respectively. The protein is shown in cartoon model in gray, whereas the residues constituting the aromatic cage are shown in stick model. The nitrogen and oxygen atoms are in blue and red, respectively, whereas the carbon atoms of the residues and the ligands are in green and cyan, respectively. The hydrogen bonds between the cationic center and the Trp149 backbone oxygen are labeled by black lines. (For interpretation of the references to color in this figure legend, the reader is referred to the web version of the article.)

nAChR) at clinical concentrations [65]. Both agonists and competitive antagonists of nAChRs have potential analgesic activities. ABT-366833, ABT-202 and ABT-894 are all agonists for different nAChR subtypes, which are under development for use as analgesics [66]. Therefore, the compounds that have anesthetic or analgesic activities likely interact with the α7 nAChR, and further experimental investigations may be necessary.

3.3.2. Interactions between docked compounds and α7 nAChR

We manually examined the docked conformations of the screened compounds and the interactions between the representative compounds and α7 nAChR and determined the following: the docked compounds were located in the aromatic cage of the binding site (Fig. 8A) with their structures extending toward the complementary component in a similar direction as the pyridine ring of nicotine (compare Figs. 1C and 8A). They formed extensive interactions with the residues constituting the binding cavity, particularly the aromatic cage (Fig. 8A). These included hydrophobic interactions between the aromatic residues and the compounds' hydrophobic groups, electrostatic interactions that are known as cation–π interactions, and hydrogen-bond interactions. Because hydrogen bonds between the agonist and Trp149 backbone oxygen were used to screen the compounds, the cationic centers of these compounds were in close proximity to the Trp149 oxygen, and this hydrogen-bonding pattern was conserved among them. There were also other hydrogen bonds between the ligands and receptor; however, no consistent hydrogen bond interactions were found in relation to their structural diversities.

The binding conformations of compounds 18 and 60 are shown in Figs. 8B and C, respectively, as examples of docking conformations. In compound 18 (Fig. 8B), a piperidine ring is connected to a cyclohexane ring through a dioxolan and flexible chain. The cationic center of the piperidine ring forms cation–π interactions and hydrogen bonds with the aromatic cage, whereas the cyclohexane extends toward the Trp55 and forms π–π interactions with its side chain. There are also possible hydrogen bonds between the oxygen atoms of the dioxolan and Trp192 backbones. The binding pose of compound 60 (Fig. 8C) is very similar to that of compound 18. The aforementioned binding conformations and interactions, particularly the role of the aromatic cage, are highly consistent with the interactions that are found in the agonist-AChBP complex crystal structures, supporting the validity of our simulations.

4. Conclusion

We applied various molecular modeling techniques, including homology modeling, molecular docking, and quantitative structure activity relationship (QSAR) analyses in the present work to virtually screen possible α7 nAChR agonists that may be used in the treatment of various neuronal disorders, particularly Alzheimer's disease.

Previous drug discovery and design studies were solely based on either docking simulations or QSAR studies; however, our study has combined docking calculations, molecular feature searches, hydrogen bond analyses, and QSAR modeling. Additionally, we used a very simple model containing only two molecular features (a cationic center and hydrogen bond acceptor) (Figs. 1 and 2) and hydrogen bond analyses to aid in our screening before and after the docking simulations, respectively. Although the molecular features and structural analysis used in our simulations were very simple, they not only reduced the number of docked compounds and computational costs but also increased the accuracy of the virtual screening method and reliability of our results. To the best of our knowledge, this is the first use of biological knowledge regarding agonist-nAChR interactions in virtual screening applications.

Our new QSAR studies verified the accuracy of our virtual screening method and reliability of the screened results. The QSAR model also provided a novel understanding of the properties affecting the ligand recognition. The significance of the positive polar VDW surface area (PEOE_VSA_PPOS) is due to the electrostatic interactions between the agonist's cationic center and the electron-rich aromatic cage of the binding site [18]. The SlogP_VSA1 highlighted

the importance of the carbon atoms connecting to the cationic center which interacts with the hydrophobic aromatic residues [67]. The molecular descriptors also revealed that the molecular topologies (Zagreb index and Kier2) are related to the agonist recognition, which has not been previously reported. These results imply that the molecular flexibility, degree of branching and overall shape may be considered in future drug design studies.

As an alternative to the costly task of drug screening by experimental methods, our molecular modeling studies have provided a novel, reliable and low cost computational method for the virtual screening of nAChR agonists.

Although our study has provided novel chemical structures that are likely to interact with the agonist sites of nAChRs, we would like to note that binding at the agonist site does not lead to the invocation of ion flux through the nAChRs. Agonist binding at the extracellular domains of nAChRs triggers conformational changes in the vicinities of the binding cavities; they are then transferred to the transmembrane domains and induce conformational changes to the transmembrane helices constituting the channel pores, ultimately resulting in ion flux through the channels. Some of the compounds that were reported in the current study may have high affinities with the agonist sites but may not produce these structural changes. It will be necessary to perform experimental studies to ensure the affinities and identify the agonist compounds in addition to those that behave like antagonists [68]. Our results may be used in future experiments to investigate the interactions of the compounds with nAChRs or may be used in *in vivo* experiments to test their effects on the memory abilities of animal models.

Acknowledgements

This work is supported by grants from the National High-Tech R&D Program (863 Program Contract No. 2012AA020307), the National Basic Research Program of China (973 Program) (Contract No. 2012CB721000), and the Key Project of Shanghai Science and Technology Commission (Contract No. 11JC1406400), which were awarded to D.Q. Wei.

Appendix A. Supplementary data

Supplementary data associated with this article can be found, in the online version, at http://dx.doi.org/10.1016/j.jmgm.2012.11.008.

References

[1] D.A. Snowdon, L.H. Greiner, J.A. Mortimer, K.P. Riley, P.A. Greiner, W.R. Markesbery, Brain infarction and the clinical expression of Alzheimer disease, Journal of the American Medical Association 277 (1997) 813.
[2] T. Babic, The cholinergic hypothesis of Alzheimer's disease: a review of progress, Journal of Neurology, Neurosurgery and Psychiatry 67 (1999) 558.
[3] A. Nordberg, Nicotinic receptor abnormalities of Alzheimer's disease: therapeutic implications, Biological Psychiatry 49 (2001) 200–210.
[4] J. Hardy, D.J. Selkoe, The amyloid hypothesis of Alzheimer's disease: progress and problems on the road to therapeutics, Science 297 (2002) 353.
[5] B. Buisson, D. Bertrand, Nicotine addiction: the possible role of functional upregulation, Trends in Pharmacological Sciences 23 (2002) 130–136.
[6] R.S. Hurst, M. Hajós, M. Raggenbass, T.M. Wall, N.R. Higdon, J.A. Lawson, et al., A novel positive allosteric modulator of the α7 neuronal nicotinic acetylcholine receptor: in vitro and in vivo characterization, Journal of Neuroscience 25 (2005) 4396–4405.
[7] R. Felix, E.D. Levin, Nicotinic antagonist administration into the ventral hippocampus and spatial working memory in rats, Neuroscience 81 (1997) 1009–1017.
[8] S. Georgi, Nicotinic acetylcholine receptors and Alzheimer's disease therapeutics: a review of current literature, Journal of Young Investigator 12 (2005).
[9] J. Toyohara, K. Hashimoto, α7 nicotinic receptor agonists: potential therapeutic drugs for treatment of cognitive impairments in schizophrenia and Alzheimer's disease, The Open Medicinal and Chemistry Journal 4 (2010) 37.
[10] A.H. Rezvani, E. Kholdebarin, F.H. Brucato, P.M. Callahan, D.A. Lowe, E.D. Levin, Effect of R3487/MEM3454 a novel nicotinic [alpha] 7 receptor partial agonist and 5-HT3 antagonist on sustained attention in rats, Progress in Neuropsychopharmacology and Biological Psychiatry 33 (2009) 269–275.
[11] S.N. Haydar, J. Dunlop, Neuronal nicotinic acetylcholine receptors-targets for the development of drugs to treat cognitive impairment associated with schizophrenia and Alzheimers disease, Current Topics in Medicinal Chemistry 10 (2010) 144–152.
[12] D. Feuerbach, K. Lingenhoehl, H.R. Olpe, A. Vassout, C. Gentsch, F. Chaperon, et al., The selective nicotinic acetylcholine receptor [alpha] 7 agonist JN403 is active in animal models of cognition, sensory gating, epilepsy and pain, Neuropharmacology 56 (2009) 254–263.
[13] M.B. Marrero, R.L. Papke, B.S. Bhatti, S. Shaw, M. Bencherif, The neuroprotective effect of 2-(3-pyridyl)-1-azabicyclo [3,2,2] nonane (TC-1698), a novel α7 ligand, is prevented through angiotensin II activation of a tyrosine phosphatase, Journal of Pharmacology and Experimental Therapeutics 309 (2004) 16.
[14] F.G. Boess, J. De Vry, C. Erb, T. Flessner, M. Hendrix, J. Luithle, et al., The novel α7 nicotinic acetylcholine receptor agonist N-[(3R)-1-azabicyclo [2.2 2] oct-3-yl]-7-[2-(methoxy) phenyl]-1-benzofuran-2-carboxamide improves working and recognition memory in rodents, Journal of Pharmacology and Experimental Therapeutics 321 (2007) 716.
[15] N. Unwin, Refined structure of the nicotinic acetylcholine receptor at 4 Å resolution, Journal of Molecular Biology 346 (2005) 967–989.
[16] K. Brejc, W.J. van Dijk, R.V. Klaassen, M. Schuurmans, J. van der Oost, A.B. Smit, et al., Crystal structure of an ACh-binding protein reveals the ligand-binding domain of nicotinic receptors, Nature 411 (2001) 269–276.
[17] D.C. Chiara, Y. Xie, J.B. Cohen, Structure of the agonist-binding sites of the Torpedo nicotinic acetylcholine receptor: affinity-labeling and mutational analyses identify γTyr-111/δArg-113 as antagonist affinity determinants, Biochemistry 38 (1999) 6689–6698.
[18] R.X. Gu, Y.Q. Zhong, D.Q. Wei, Structural basis of agonist selectivity for different nAChR subtypes: insights from crystal structures, mutation experiments and molecular simulations, Current Pharmaceutical Design 17 (2011) 1652–1662.
[19] P.H.N. Celie, S.E. van Rossum-Fikkert, W.J. Van Dijk, K. Brejc, A.B. Smit, T.K. Sixma, Nicotine and carbamylcholine binding to nicotinic acetylcholine receptors as studied in AChBP crystal structures, Neuron 41 (2004) 907–914.
[20] X. Xiu, N.L. Puskar, J.A.P. Shanata, H.A. Lester, D.A. Dougherty, Nicotine binding to brain receptors requires a strong cation–π interaction, Nature 458 (2009) 534–537.
[21] C. Ulens, A. Akdemir, A. Jongejan, R. van Elk, S. Bertrand, A. Perrakis, et al., Use of acetylcholine binding protein in the search for novel α7 nicotinic receptor ligands. in silico docking, pharmacological screening, and X-ray analysis, Journal of Medicinal Chemistry 52 (2009) 2372–2383.
[22] X. Huang, F. Zheng, X. Chen, P.A. Crooks, L.P. Dwoskin, C.G. Zhan, Modeling subtype-selective agonists binding with α4β2 and α7 nicotinic acetylcholine receptors: effects of local binding and long-range electrostatic interactions, Journal of Medicinal Chemistry 49 (2006) 7661–7674.
[23] R. Rodriguez, G. Chinea, N. Lopez, T. Pons, G. Vriend, Homology modeling, model and software evaluation: three related resources, Bioinformatics 14 (1998) 523.
[24] M. Kuhn, C. Von Mering, M. Campillos, L.J. Jensen, P. Bork, STITCH: interaction networks of chemicals and proteins, Nucleic Acids Research 36 (2008) D684–D688.
[25] C.G. Wermuth, C.R. Ganellin, P. Lindberg, L.A. Mitscher, Glossary of terms used in medicinal chemistry (IUPAC recommendations 1997), Annual Reports in Medicinal Chemistry 33 (1998) 385–395.
[26] G. Wolber, T. Seidel, F. Bendix, T. Langer, Molecule-pharmacophore superpositioning and pattern matching in computational drug design, Drug Discovery Today 13 (2008) 23–29.
[27] C.A. Lipinski, F. Lombardo, B.W. Dominy, P.J. Feeney, Experimental, computational approaches to estimate solubility and permeability in drug discovery and development settings, Advanced Drug Delivery Reviews 23 (1997) 3–25.
[28] C.A. Lipinski, Lead-and drug-like compounds: the rule-of-five revolution, Drug Discovery Today: Technology 1 (2004) 337–341.
[29] M. Vieth, J.J. Sutherland, Dependence of molecular properties on proteomic family for marketed oral drugs, Journal of Medicinal Chemistry 49 (2006) 3451–3453.
[30] D.A. Gschwend, A.C. Good, I.D. Kuntz, Molecular docking towards drug discovery, Journal of Molecular Recognition 9 (1996) 175–186.
[31] G.M. Morris, R. Huey, W. Lindstrom, M.F. Sanner, R.K. Belew, D.S. Goodsell, et al., AutoDock4 and AutoDockTools4: automated docking with selective receptor flexibility, Journal of Computational Chemistry 30 (2009) 2785–2791.
[32] R.X. Gu, H. Gu, Z.Y. Xie, J.F. Wang, H.R. Arias, D.Q. Wei, et al., Possible drug candidates for Alzheimers disease deduced from studying their binding interactions with 7 nicotinic acetylcholine receptor, Medicinal Chemistry 5 (2009) 250–262.
[33] H.R. Arias, R.X. Gu, D. Feuerbach, D.Q. Wei, Different interaction between the agonist JN403 and the competitive antagonist methyllycaconitine with the human α7 nicotinic acetylcholine receptor, Biochemistry 49 (2010) 4169–4180.
[34] K.C. Chou, Insights from modelling the 3D structure of the extracellular domain of [alpha] 7 nicotinic acetylcholine receptor, Biochemical and Biophysical Research Communications 319 (2004) 433–438.
[35] S.B. Hansen, G. Sulzenbacher, T. Huxford, P. Marchot, P. Taylor, Y. Bourne, Structures of Aplysia AChBP complexes with nicotinic agonists and antagonists reveal distinctive binding interfaces and conformations, EMBO Journal 24 (2005) 3635–3646.
[36] H.R. Arias, R.X. Gu, D. Feuerbach, B.B. Guo, Y. Ye, D.Q. Wei, Novel positive allosteric modulators of the human α7 nicotinic acetylcholine receptor, Biochemistry 50 (2011) 5263–5278.

[37] Y.H. Zhao, J. Le, M.H. Abraham, A. Hersey, P.J. Eddershaw, C.N. Luscombe, et al., Evaluation of human intestinal absorption data and subsequent derivation of a quantitative structure–activity relationship (QSAR) with the Abraham descriptors, Journal of Pharmaceutical Sciences 90 (2001) 749–784.
[38] B.A. Acker, E.J. Jacobsen, B.N. Rogers, D.G. Wishka, S.C. Reitz, D.W. Piotrowski, et al., Discovery of N-[(3R, 5R)-1-azabicyclo [3.2 1] oct-3-yl] furo [2,3-c] pyridine-5-carboxamide as an agonist of the [alpha] 7 nicotinic acetylcholine receptor: in vitro and in vivo activity, Bioorganic and Medicinal Chemistry Letters 18 (2008) 3611–3615.
[39] D.J. Anderson, W.H. Bunnelle, B.W. Surber, J. Du, C.S. Surowy, E. Tribollet, et al., [3H] A-585539 a novel high affinity α7 neuronal nicotinic receptor agonist: radioligand binding characterization to rat and human brain, Journal of Pharmacology and Experimental Therapeutics 324 (2007) 179–187.
[40] M. Ding, S. Ghanekar, C.S. Elmore, J.R. Zysk, J.L. Werkheiser, C.M. Lee, et al., [3H] Chiba-1001 (methyl-SSR180711) has low in vitro binding affinity and poor in vivo selectivity to nicotinic alpha-7 receptor in rodent brain, Synapse 66 (2012) 315–322.
[41] J.C. Gordon, E. Phillips, D.A. Gurley, J.R. Heys, L.A. Lazor, H.G. Barthlow, et al., In vitro binding characteristics of [3H] AZ11637326 a novel [alpha] 7-selective neuronal nicotinic receptor agonist radioligand, European Journal of Pharmacology 645 (2010) 63–69.
[42] T.A. Hauser, A. Kucinski, K.G. Jordan, G.J. Gatto, S.R. Wersinger, R.A. Hesse, et al., TC-5619: an alpha7 neuronal nicotinic receptor-selective agonist that demonstrates efficacy in animal models of the positive and negative symptoms and cognitive dysfunction of schizophrenia, Biochemical Pharmacology 78 (2009) 803–812.
[43] A. Mazurov, J. Klucik, L. Miao, T.Y. Phillips, A. Seamans, J.D. Schmitt, et al., 2-(Arylmethyl)-3-substituted quinuclidines as selective α7 nicotinic receptor ligands, Bioorganic and Medicinal Chemistry Letters 15 (2005) 2073–2077.
[44] A.A. Mazurov, J.D. Speake, D. Yohannes, Discovery and development of α7 nicotinic acetylcholine receptor modulators, Journal of Medicinal Chemistry 54 (2011) 7943–7961.
[45] L. Munoz, Novel nicotinic acetylcholine receptor ligands based on cytisine and choline, Universitäts-und Landesbibliothek Bonn (2005).
[46] R. Tatsumi, M. Fujio, H. Satoh, J. Katayama, S. Takanashi, K. Hashimoto, et al., Discovery of the α7 nicotinic acetylcholine receptor agonists. (R)-3′-(5-chlorothiophen-2-yl) spiro-1-azabicyclo [2,2,2] octane-3,5′-[1′,3′] oxazolidin-2′-one as a novel, potent, selective, and orally bioavailable ligand, Journal of Medicinal Chemistry 48 (2005) 2678–2686.
[47] R. Tatsumi, M. Fujio, S. Takanashi, A. Numata, J. Katayama, H. Satoh, et al., (R)-3′-(3-Methylbenzo [b] thiophen-5-yl) spiro [1-azabicyclo [2,2,2] octane-3, 5′-oxazolidin]-2′-one, a Novel and Potent α7 nicotinic acetylcholine receptor partial agonist displays cognitive enhancing properties, Journal of Medicinal Chemistry 49 (2006) 4374–4383.
[48] I. Guyon, A. Elisseeff, C. Aliferis, Causal feature selection, in: Computational Methods of Feature Selection, Data Mining and Knowledge Discovery Series Chapman and Hall/CRC, Boca Raton, London, New York, 2007, pp. 63–85.
[49] M.A. Hall, Correlation-based Feature Selection for Machine Learning, The University of Waikato, Hamilton, New Zealand, 1999.
[50] R. Kohavi, G.H. John, Wrappers for feature subset selection, Artificial Intelligence 97 (1997) 273–324.
[51] D.E. Goldberg, Genetic algorithms in search, optimization, and machine learning, Addison-Wesley (1989) 15.
[52] A. Smola, V. Vapnik, Support vector regression machines, Advances in Neural Information Processing Systems 9 (1997) 155–161.
[53] J.H. Holland, Adaptation in Natural and Artificial Systems, University of Michigan Press, Ann Arbor, MI, 1975.
[54] M.L. Raymer, W.E. Punch, E.D. Goodman, L.A. Kuhn, A.K. Jain, Dimensionality reduction using genetic algorithms, IEEE Transactions on Evolutionary Computation 4 (2000) 164–171.
[55] C. Cortes, V. Vapnik, Support-vector networks, Machine Learning 20 (1995) 273–297.
[56] N. Cristianini, J. Shawe-Taylor., An Introduction to Support Vector Machines and Other Kernel-based Learning Methods, Cambridge University Press, Cambridge, England, 2000.
[57] H. Drucker, C.J.C. Burges, L. Kaufman, A. Smola, V. Vapnik, Support vector regression machines, Advances in Neural Information Processing Systems 9 (1997) 155–161.
[58] M.D. Buhmann, Radial Basis Functions: Theory and Implementations, Cambridge University Press, Cambridge, England, 2003.
[59] K.C. Chou, D.Q. Wei, W.Z. Zhong, Binding mechanism of coronavirus main proteinase with ligands and its implication to drug design against SARS, Biochemical and Biophysical Research Communications 308 (2003) 148–151.
[60] K.C. Chou, Energy-optimized structure of antifreeze protein and its binding mechanism, Journal of Molecular Biology 223 (1992) 509–517.
[61] K.C. Chou, Insights from modeling the tertiary structure of human BACE2, Journal of Proteome Research 3 (2004) 1069–1072.
[62] S. Prasanna, E. Manivannan, S.C. Chaturvedi, Quantitative structure–activity relationship analysis of a series of 2,3-diaryl benzopyran analogues as novel selective cyclooxygenase-2 inhibitors, Bioorganic and Medicinal Chemistry Letters 14 (2004) 4005–4011.
[63] B. Zhou, I. Gutman, Relations between Wiener hyper-Wiener and Zagreb indices, Chemical Physics Letters 394 (2004) 93–95.
[64] L. Xue, J. Bajorath, Molecular descriptors in chemoinformatics computational combinatorial chemistry and virtual screening, Combinatorial Chemistry and High Throughput Screening 3 (2000) 363–372.
[65] E. Tassonyi, E. Charpantier, D. Muller, L. Dumont, D. Bertrand, The role of nicotinic acetylcholine receptors in the mechanisms of anesthesia, Brain Research Bulletin 57 (2002) 133–150.
[66] K.K. Jain, Modulators of nicotinic acetylcholine receptors as analgesics, Current Opinion Investigation and drugs 5 (2004) 76.
[67] C. Binda, P. Newton-Vinson, F. Hubálek, D.E. Edmondson, A. Mattevi, Structure of human monoamine oxidase B a drug target for the treatment of neurological disorders, Nature Structural and Molecular Biology 9 (2001) 22–26.
[68] M.P. Tang, Z.X. Wang, Y. Zhou, W. Xu, S.T. Li, L.Y. Wang, D.Q. Wei, Z.D. Qiao, A novel drug candidate for Alzheimer disease treatment – gx-50 derived from Zanthoxylum Bungeanum. Journal of Alzheimer's Disease, in press.
[69] L.H. Hall, L.B. Kier, The molecular connectivity chi indexes and kappa shape indexes in structure-property modeling, Reviews in Computational Chemistry (1991) 367–422.
[70] S.A. Wildman, G.M. Crippen, Prediction of physicochemical parameters by atomic contributions, Journal of Chemical Information and Computer Science 39 (1999) 868–873.